ADVANCED OPTICAL MATERIALS
www.advopticalmat.de

Enhancing Triplet Excitons Lifetime Through Controlled Intermolecular Interactions

*Martin Richter, Muhammed Jeneesh Kariyottukuniyil, Zhiyun Xu, Philipp Ludwig, Pavel V. Kolesnichenko, Christian Huck, Uwe H. F. Bunz, Christof Wöll, Wolfgang Wenzel, and Petra Tegeder**

Singlet fission (SF) is a process in which a singlet exciton is converted into two triplet excitons, significantly enhancing charge generation in organic solar cells. It has been shown that the rate of SF and the lifetime of the generated triplet excitons strongly depend on the molecular arrangement. In this work, a cofacial orientation of pentacene molecules is achieved by embedding organic linkers containing pentacene in a surface-anchored metal–organic framework. Transient absorption spectroscopy and a quantum mechanical analysis are used to analyze the exciton dynamics in a broad spectral range from near-ultraviolet to near-infrared. The observed spectra indicate that a singlet excited state generates a correlated triplet pair within a few picoseconds. Subsequent dynamics show the formation of long-lived excitons (39 µs) with triplet character. This exceeds by far the observed lifetime of triplet excitons generated in pentacene thin films and may enhance triplet exciton harvesting capabilities in photovoltaic cells.

1. Introduction

The interest in the use of solar energy has increased significantly in the last decade. Exploitation of singlet fission (SF) promises to increase the efficiency of photovoltaic junctions up to 44%, which surpasses the Shockley–Queisser limit.[1,2] In SF materials, a singlet (S) exciton is converted into two lower-energy triplet (T) excitons ($E_{S1} \approx 2E_{T1}$). The efficiency of a solar cell could thus be enhanced if the triplet state energy is comparable to the semiconductor band gap, provided that the energy can be transferred. Using this process, high-energy photons can be utilized, whose energy would otherwise be lost in dissipative processes. In addition to fast SF and high triplet quantum yield (TQY), a long lifetime of the generated triplet excitons is of great importance, since it increases the probability of harvesting the charge carriers.

Charge-transfer (CT) states occur in a direct or indirect manner and especially the multiexcitonic state ^{m}(TT) plays a key role in the SF process.[3–7] Here, ^{m}(TT) specifies a coherent state of triplets on adjacent chromophores both in an excited triplet state. The four electrons involved in this process spin-couple to have a multiplicity of $m = 1$, 3or5. The spin-coupled state must retain spin multiplicity m = 1 initial to the generation of the triplet pair to ensure conservation of angular momentum. Many studies report the following model for SF:[8–10]

$$(S_0S_1) \xrightarrow{(1)} {}^{1}(T_1T_1) \xrightarrow{(2)} {}^{1}(T_1 \cdots T_1) \xrightarrow{(3)} 2T_1 \quad (1)$$

where (S_0S_1) indicates a singlet excitation on one of the two chromophores, $^{1}(T_1 \cdots T_1)$ describes a spin-coupled triplet pair that is spatially separated and has lost electronic coherence, and $2T_1$ are two uncoupled triplet excitons. The rate of the first step – the triplet-pair generation – is extremely fast with 70–100 fs in pentacene (PEN) thin films.[11] The second and third steps are more elusive, and an unambiguous assignment of kinetic rates is difficult. Some studies report the rate of the second step on the ps-ns time scale for PEN derivatives.[8,12] Spatially separated triplet excitons have been reported to give a photo-induced absorption (PIA) shifted to lower energies.[8,13] The

M. Richter, P. V. Kolesnichenko, C. Huck, P. Tegeder
Physikalisch-Chemisches Institut
Ruprecht-Karls-Universität Heidelberg
Im Neuenheimer Feld 253/229, 69120 Heidelberg, Germany
E-mail: tegeder@uni-heidelberg.de
M. J. Kariyottukuniyil, W. Wenzel
Institut für Nanotechnologie
Karlsruher Institut für Technologie
Hermann-von-Helmholtz-Platz 1, 76131 Karlsruhe, Germany
Z. Xu, C. Wöll
Institut für Funktionelle Grenzflächen
Karlsruher Institut für Technologie
Hermann-von-Helmholtz-Platz 1, 76131 Karlsruhe, Germany
P. Ludwig, U. H. F. Bunz
Organisch-Chemisches Institut
Ruprecht-Karls-Universität Heidelberg
Im Neuenheimer Feld 271, 69120 Heidelberg, Germany
P. V. Kolesnichenko
Institute for Molecular Systems Engineering and Advanced Materials
Ruprecht-Karls-Universität Heidelberg
Im Neuenheimer Feld 225, 69120 Heidelberg, Germany

The ORCID identification number(s) for the author(s) of this article can be found under https://doi.org/10.1002/adom.202502979

DOI: 10.1002/adom.202502979

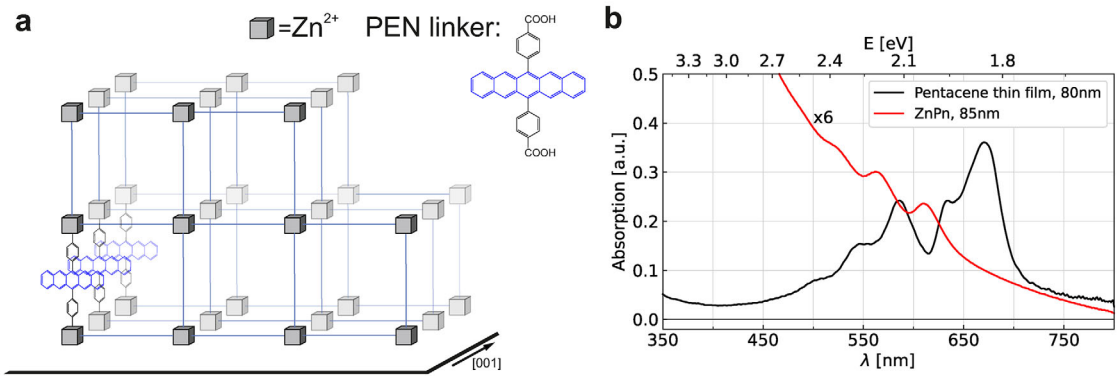

Figure 1. Structure and optical properties of ZnPn a) Schematic of the ZnPn SURMOF structure. Blue lines indicate the PEN linkers. Adaptation from ref.[21]. b) UV/Vis absorption spectra of PEN thin film (black) and ZnPn (red) on quartz substrates.

overall lifetime of the triplet excitons in PEN thin films is more well-founded with a few nanoseconds.[14] For the above mechanism the following criteria are crucial: (1) energy level matching at the single molecular level: $E_{S_1} \geq 2E_{T_1}$ and $E_{T_2} \geq 2E_{T_1}$,[15] which ensures that the splitting of a singlet excitation into two triplet excitons is thermodynamically feasible, while triplet-triplet annihilation (TTA) is not; (2) strong electronic coupling between molecular aggregates, i.e., $S_0S_1 \rightarrow {}^1(T_1T_1)$[16] and (3) efficient separation dynamics, meaning that the correlated triplet pair ${}^1(T_1T_1)$ evolves into two independent triplet excitons $2T_1$ that can physically separate from each other.[17,18] These are referred to as (1) energetic, (2) coupling, and (3) separation criteria, respectively.

Lubert–Perquel et al.[4] proposed that a parallel orientation of the chromophores favours the formation of free separated triplet excitons. In addition, the displacement along the long molecular axis Δx in a slip-stacked configuration is also of crucial importance. Pensack et al.[19] reported that when $\Delta x = 0$ the TQY is suppressed.

Here, we investigate PEN embedded in a surface-anchored metal-organic framework (SURMOF), see **Figure 1a** and compare it to a PEN thin film. In the thin film the herringbone structure is adopted (compare Figure 5b). The PEN linker in the MOF forms a coordination bond with the Zn^{2+} dimer nodes, creating a parallel orientation with $\Delta x \neq 0$. This sample is denoted by ZnPn with Zn referring to zinc and Pn to pentacene. The difference in geometry compared to the PEN thin film has an enormous impact on both the observed dynamics and electronic properties. The geometry provides 1D channels for charge transport, which may also favour the separation of triplet pairs. In addition, anchoring at the surface produces a high crystalline order and also facilitates attaching electrical contacts for device applications in comparison to a MOF powder.[20] Regarding the SF properties, the sample exhibits extraordinarily long triplet exciton lifetimes compared to other bulk materials with PEN as SF chromophore, which is beneficial for light harvesting devices. At the same time, the slowdown in triplet exciton generation is less drastic. Additionally, the prominent triplet-pair absorption of the PEN thin film in the near-infrared (NIR) spectral region is almost absent in the ZnPn.

2. Results and Discussion

2.1. Coupling in the Ground State

The UV/Vis absorption spectra of ZnPn compared to a PEN thin film on a glass substrate are shown in Figure 1b. The $S_0 \rightarrow S_1$ transition in the PEN thin film, shows Davydov splitting with absorption maxima at 670 and 632 nm.[22–24] Furthermore, peaks at 585, 545 and 500 nm are observed, which stem from a vibronic progression or CT transitions.[22,25] In contrast to the thin film, the ZnPn sample does not show Davydov splitting – a vibronic progression with blue-shifted maxima at 525, 565 and 610 nm is observed instead.

We attribute the lack of Davydov splitting to the different geometry of the unit cell. X-ray diffraction measurements[21] led to the conclusion that ZnPn adopts a structure of type MOF-2, which consists of 2D layers as illustrated in Figure 1a. Because this structure can only be achieved with a correct placement of the organic PEN linkers between the Zn^{2+} dimers, and considering the geometric constraints as well as the spectroscopic evidence for PEN chromophores in the sample, a cofacial orientation appears highly likely. As in the PEN thin film, there are two molecules in a unit cell, but in ZnPn they are separated by the Zn-oxo-metal node. The lack of splitting indicates that there is no significant coupling across the nodes. However, there is a substantial coupling between the PEN linkers in [001] direction expected, since a redshift of 50 meV[21] compared to linkers in solution was found. From our calculations we can confirm the energetic requirements $E_{S_1} \geq 2E_{T_1}$ and $E_{T_2} \geq 2E_{T_1}$ for SF. For the pentacene molecule time-dependent density functional theory (TD-DFT) calculations yield $E_{S1} = 1.81$ eV, $E_{T1} = 0.69$ eV and $E_{T2} = 1.92$ eV. For the pentacene linker in the MOF the corresponging energis are $E_{S1} = 1.85$ eV, $E_{T1} = 0.62$ eV and $E_{T2} = 1.93$ eV.

2.2. Triplet Formation Dynamics

First, we will revisit the characteristic features of the PEN thin films. The corresponding femtosecond transient absorption (fs-TA) spectra are shown in **Figure 2a**. The ground state bleach (GSB) is located at 670 nm and the bleach at 584 nm likely stems from a vibronic sideband.[26,27] The broad positive

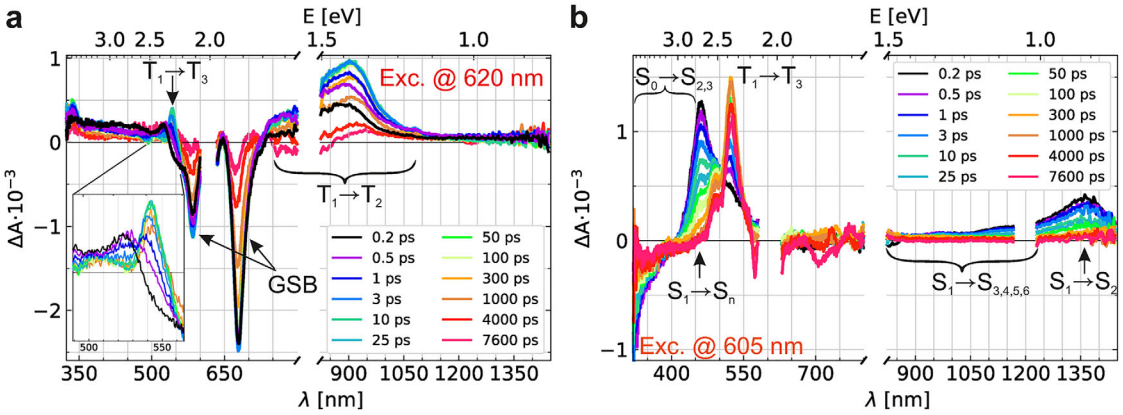

Figure 2. Excited state dynamics of PEN thin films and ZnPn a) fs-TA spectra of PEN thin film excited at 620 nm. The spectrum in the visible was probed at 50° angle of incidence (424 μJ/cm^2) and the NIR spectrum at 0° (495 μJ/cm^2). The inset shows the $T_1 \rightarrow T_3$ PIA. b) fs-TA spectra of ZnPn excited at 605 nm (424 μJ/cm^2).

signal ranging from 750 to 1050 nm is associated with the $T_1 \rightarrow T_2$ transition,[11,26,28,29] which has been suggested to be enhanced in the solid state compared to PEN in solution.[26] The $T_1 \rightarrow T_3$ transition can be observed at 540 nm and becomes stronger when the probe beam is not orthogonal to the sample surface[28,30] (see also Figure S2, Supporting Information). This indicates that the transition dipole moment, which is aligned with the long molecular axis, is orthogonal to the sample surface. This PIA is delayed and has a rise time of ≈1 ps.[30] Interestingly, in addition to the known $T_1 \rightarrow T_3$ and $T_1 \rightarrow T_2$ transitions, we also observe a PIA centred at 340 nm. To our knowledge, this PIA has not been detected with TA before. We attribute it to a triplet-triplet transition as outlined in the Supporting Information (see also Figures S1 and S2, Supporting Information for more information).

The ZnPn TA spectra are shown in Figure 2b after excitation with light at 605 nm. It is evident that the TA data do not resemble those of the thin film, but the spectral features are fairly well-known for PEN in solution.[31–36] Most prominently, a transformation of the initially formed PIA peaking at 460 nm to a state with maximum absorption at 525 nm is apparent. We attribute the PIA centred ≈460 nm to a $S_1 \rightarrow S_n$ transition and the PIA at 525 nm to $T_1 \rightarrow T_3$ in accordance with literature.[34–39] Furthermore, a broad PIA can be observed in the NIR region, with the main absorption at 1360 nm corresponding to the $S_1 \rightarrow S_2$ transition, based on our calculations. The strongly correlated decay of the PIAs at 460 and 1360 nm (Figure S7, Supporting Information) also confirms that these spectra originate from the same states. This is also verified by global analysis (GA), see Figure S12 (Supporting Information). The PIA between 700 and 1000 nm is the most prominent sign of triplet excitons in the PEN thin film, and a corresponding signal can not be identified in ZnPn for an excitation wavelength of 605 nm. In the range from 900 to 1100 nm a weak absorption can be seen for ZnPn. Nonetheless, it shows the same dynamics as the feature at 1360 nm, and according to our calculations, it is likely that it corresponds to excitations to higher singlet states (compare Table S2, Supporting Information). Previous calculations on a PEN dimer in face-to-face orientation predict a weak PIA from triplet excitons in this spectral region and enhanced intensity with increasing intermolecular coupling.[7] For higher excitation energies (355 nm) we observe a weak PIA that outlasts the singlet PIA.

Our measured values for fs-TA can be well modeled with three sequential exponential functions. The obtained evolution associated difference spectra (EADS) are shown in **Figure 3**a. The near-isosbestic point at 500 nm indicates that the sequential model is a valid approximation. We attribute the first EADS, emerging immediately after excitation to the singlet excited state (S_0S_1) due to its main absorption at 460 nm. It decays with a time constant of ≈4.9 ps into a state showing characteristics of both singlet and triplet excited state absorption. Therefore, we attribute the second EADS to the $^1(T_1T_1)$ intermediate state. The decay at 460 nm and concomitant rise of the triplet exciton signature at 525 nm can be clearly seen in Figure 3b. It has been proposed that the $^1(T_1T_1)$ state exhibits spectral features of both species.[40,41] Therefore, the rate of triplet-pair generation is on the order of a few picoseconds (4.9 ps) in ZnPn and 70—100 fs in the PEN thin film. The comparative slowdown in this rate is most likely explained by a weaker electronic coupling in ZnPn, which in turn results from a higher CT state energy, as obtained from calculations (see below). Ritesh et al.[21] have shown that the SURMOF structure allows for frustrated rotations, and hence a fluctuating electronic coupling is possible. From the analysis we conclude that the $^1(T_1T_1)$ state decays with a time constant of ≈119 ps. For a selection of PEN derivatives the decay of the $^1(T_1T_1)$ state has been observed to be ≈1 ps,[8] thus further confirming slower dynamics in ZnPn. We would like to point out that in extended systems with heterogeneous coupling more sophisticated models have been used to describe SF.[42,43] In particular, different SF rates for the generation of the $^1(T_1T_1)$ state have been proposed, which could potentially be assigned to our observed time constants (4.9 and ≈119 ps). However, here this would imply even longer $^1(T_1T_1)$ lifetimes, which we consider unlikely, due to the large energetic splitting between the singlet and triplet states. The third EADS exhibits a vibronic structure peaking at 525 and 490 nm. We assign this spectrum to the $^m(T_1T_1)$ state. As outlined above, from the parallel alignment of the chromophores the generation of the quintet pair state is likely to be promoted.[4]

The maximum pump/probe delay possible for the fs-TA setup is 7.8 ns, therefore the third time constant is given as >8 ns, and

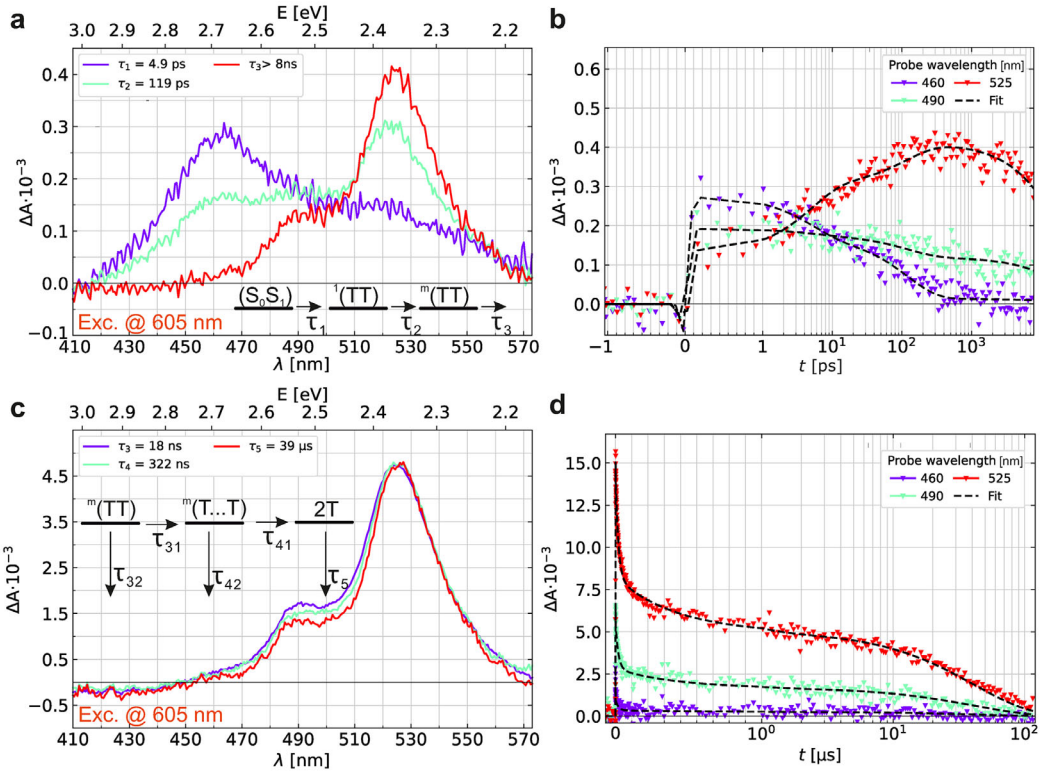

Figure 3. Global analysis of the dynamics in ZnPn. a) EADS of ZnPn excited at 605 nm (141 µJ/ cm^2). The data are fitted with three sequential exponential functions. The transient spectra are assigned to the singlet excited state (S_1S_0) (purple), the intermediate state ^{1}(TT) (green) and the triplet excited state ^{m}(TT) (red). b) Time traces of fs-TA data of ZnPn excited at 605 nm (141 µJ/ cm^2) at selected wavelengths. Data at 460 and 525 nm are associated with singlet and triplet PIA, respectively. c) SADS of fs-TA spectra of ZnPn excited at 605 nm (1132 µJ/ cm^2). The data are fitted with the kinetic model shown. d) fs-TA kinetics of ZnPn (4244 µJ/ cm^2) at selected wavelengths.

fs-TA measurements were conducted to analyze the long-lived excitations. Figure 3c,d presents the analysis on fs-TA of ZnPn after excitation at a wavelength of 605 nm. The spectra display the characteristic signature associated with triplet excitons. For describing the dynamics, the model as shown in Figure 3c is applied. The reaction ^{m}(TT)→^{m}(T...T)→2T→GS (ground state) is described by time constants $\tau_{31} = 31$ ns, $\tau_{41} = 500$ ns, and $\tau_5 = 39$ µs, along with parallel loss channels with $\tau_{32} = 43$ ns and $\tau_{42} = 920$ ns. The branching ratios in $\frac{1}{\tau_i} = \frac{1}{\tau_{i1}} + \frac{1}{\tau_{i2}} = \frac{b_i}{\tau_i} + \frac{(1-b_i)}{\tau_i}$ for $i = 3$ and 4 were optimized such, that the species associated difference spectra (SADS) are spectrally equal, since we assume that the states ^{m}(TT), ^{m}(T...T) and 2T are indistinguishable in TA experiments. Most remarkable is the long lifetime of 39 µs of the triplet excitons, which is almost four orders of magnitude larger compared to their lifetime in PEN thin films which is 10 ns.[14]

2.2.1. Fluence Dependence

Figure 4a shows kinetics of ZnPn at 460 and 525 nm, i.e. the maxima of the PIA from singlets and triplets, respectively. The data are normalised to compare the initial intensity with those at later delay times. We observed a weak PIA fluence dependence of the triplet signature (top), whereas the singlet signal (bottom) is unaffected. Faster rates with increasing fluence are detected also in PEN thin films and crystals, which has been attributed to TTA, and therefore is an indicator of free triplet excitons.[26] We indeed expect free triplet excitons, since in a highly ordered bulk structure – such as the SURMOF considered here – delocalisation and entropy are driving factors for separation.[31,44] Hence, we would argue that TTA occurs. However, the fluence dependence seems to affect only the data between tens and hundreds of picoseconds, whereas the triplet signal on the µs-scale is not affected. Considering, for example, a decrease in SF rate due to saturated sites, also fails to explain the data, since the singlet signal would then also need to be fluence dependent. Therefore we conclude that an additional decay pathway of $^1(T_1T_1)$ – which exists at this timescale – must be present. We compare different models including a bimolecular process in Figure S3 (Supporting Information), but for low fluences our model with first-order rates should be sufficient.

2.2.2. Dynamics Including Higher Excited States

To test for a dependence on the excitation wavelength, we excited the sample with 355 nm. Figure 4b shows the TA spectra for selected delays. The broad PIA, extending from the NIR to the visible range, is enhanced. In addition, the intensity at 525 nm is increased. Since the singlet and triplet PIAs overlap considerably it is much more conclusive to compare the ratio $R_{T/S}$ of the singlet and triplet absorption maxima obtained from the EADS, as listed

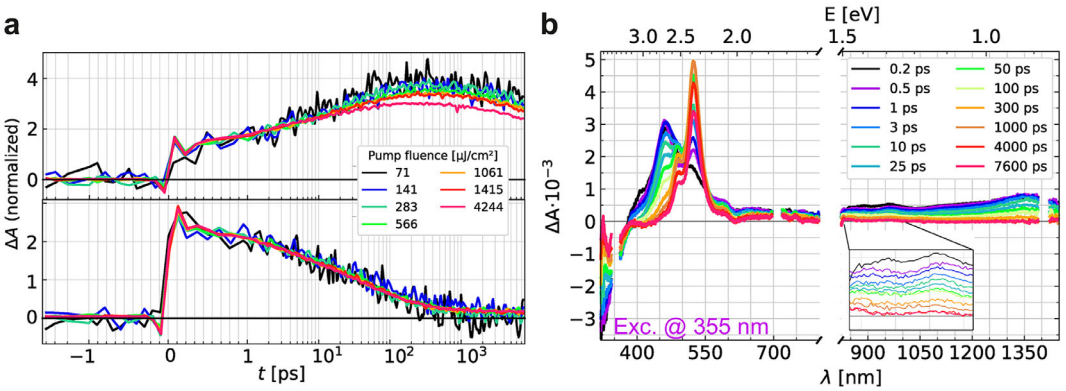

Figure 4. a) Fluence dependence of transient absorption spectra of ZnPn excited at 605 nm and probed at 525 (top) and 460 nm (bottom), which are associated with triplet and singlet exciton PIAs, respectively. b) ZnPn excited at 355 nm (141 μJ/ cm^2). The inset highlights the region where triplet-induced absorption is expected.

in **Table 1**. From the larger ratios we conclude, that the TQY is increased by ≈21% compared to an excitation with 605 nm. Furthermore, a decrease in $R_{T/S}$ with increasing fluence is apparent, which is consistent with the fluence dependence as discussed above. The broad PIA in the NIR region decays simultaneously with the PIA at 1360 nm, except for two peaks at 950 and 855 nm, which outlast it; see inset of Figure 4b. We attribute these peaks to the $T_1 \rightarrow T_2$ transition that has been missing in the spectra when exciting at 605 nm. However, there is no concomitant rise in signal intensity following the triplet feature in the visible spectral range. It has to be noted that the PEN cation also absorbs in this spectral range.[45] To compare the dynamics, kinetics with normalized intensity are shown in Figure S9 (Supporting Information). There are only slight deviations, e.g. at 460 nm, which we attribute to the difference in TQY together with the normalisation of the data. As the time evolution remains essentially the same, it suggests either that the initially excited state does not need to relax before undergoing SF, as Wilson et al.[11] have argued as well for the PEN thin film, or that the relaxation to S_1 is ultrafast.

2.3. Calculated SF Rate From Molecular Dimers and the Role of Superexchange Interactions

To elucidate the influence of the partially unresolved structure on the electro-optical properties we have undertaken a comprehensive quantum mechanical analysis of the exciton dynamics in singlet fission for both pentacene, which serves as a reference system,[46,47] and models of potential dimer configurations in the metal–organic framework. In the following, we examine the influence of different molecular structure models on the rate of singlet fission and the lifetime of triplet excitons.

Table 1. Ratio $R_{T/S}$ of maxima of EADS associated with triplet and singlet excitons obtained from the global analysis for different excitation energies and pump fluences.

λ_{ex} = 605 nm		λ_{ex} = 355 nm	
Fluence [μJ/ cm^2]	$R_{T/S}$	Fluence [μJ/ cm^2]	$R_{T/S}$
141	1.41	14	1.71
283	1.44	42	1.75
566	1.36	57	1.71
1061	1.30	89	1.71
1415	1.25	141	1.68
4244	1.12		

2.3.1. Choice of Slip-Stacked Model

A minimal morphology model comprising at least two chromophores is necessary to study the SF process. Since the geometric configuration of the MOF dimer pairs remains experimentally unavailable, we created a series of possible configurations based on the known constraints from the MOF structure, for which we performed quantum chemical calculations. The dimers in these models are placed in slip-stack configurations denoted as MOF-A, MOF-B and MOF-C (**Figure 5a**). The π-π distance $d_{\pi\pi}$ is kept constant at 3.58 Å for all dimers. The displacement Δy in the direction of the short molecular axis is initially set to Δy = 0 and the geometry optimization resulted in small displacements of Δy ~ 1.1–1.2 Å for all dimer models. The main parameter to monitor the changes in photophysical properties is the "slip" along the long molecular axis Δx. Δx has been varied from 1.81 Å for MOF-A to 6.87 Å for MOF-B and finally 9.48 Å for MOF-C. For MOF-A this results in almost face-to-face π stacked dimers. The strong interaction between the chromophores in this configuration, promotes efficient electronic coupling and charge transfer processes, facilitating rapid excitation dynamics and triplet generation. MOF-B shows face-to-face as well as edge-to-face interaction. In contrast, MOF-C exhibits the maximal stacking displacement, resulting in the least π–π interaction. Instead, edge-to-face interaction and interaction via short C···H contacts become more prominent. In the subsequent analysis, we also analyse the three known relative dimer orientations for the PEN thin film for comparison. The three dimer orientations in PEN exhibit different π–π distances and orientations resulting from variations in the relative orientation of pentacene molecules in the herringbone crystal lattice. As shown in Figure 5b, PEN-B forms a slip-stacked herringbone with π–π interactions, while the PEN-C and PEN-A dimers feature a herringbone arrangement with CH-π interactions (see also Table 2).

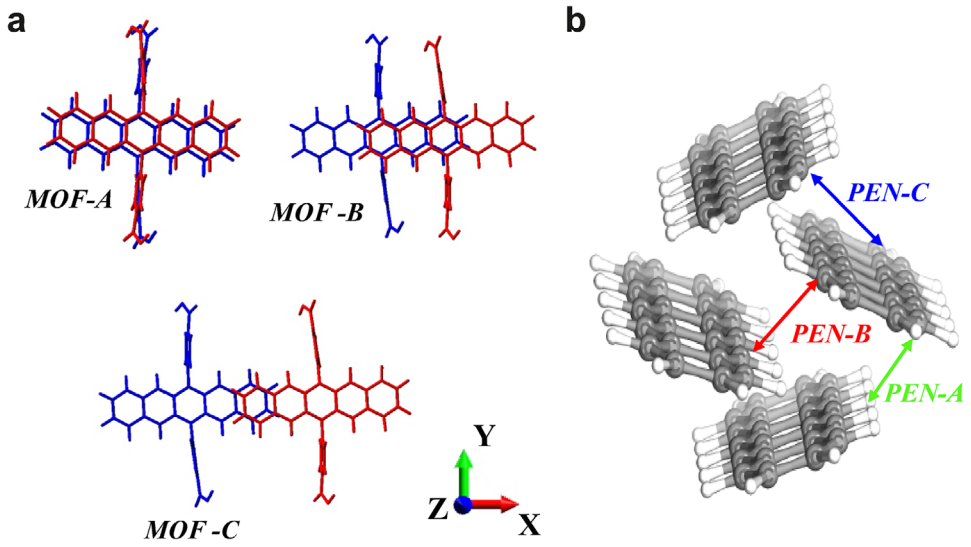

Figure 5. Dimer pair geometries considered in the computational calculations. a) The MOF-A, B and C models were constructed by placing the pentacene linkers in a coplanar geometry at a distance of 3.58 Å and then stacking both linkers with respect to the xy plane (see **Table 2**). b) The pentacene dimers PEN-A, B and C were obtained from the measured crystal structures of PEN.[48]

2.3.2. Effective-Electronic Coupling and Rate of Singlet Fission

The effective electronic couplings between the S_0S_1/S_1S_0 and the ^{1}TT states are crucial for determining the SF rate. **Table 3**, presents effective coupling energies J_{eff} for SF based on calculated coupling matrix parameters (cf. Table S3, Supporting Information). The calculations for the PEN models exhibit the largest coupling of 16.80 meV for the PEN-C model. This modulation in coupling may partly result from stacking changes imposed by the crystal structures. Notably, among the three derivatives, the calculated coupling constants are in reasonable agreement with those calculated by Chao et al.[49]

In the MOF models, the largest effective coupling associated with the least displacement along the long axis Δx (MO = 1.81, Δy = 1.21) is ≈ 21.53 meV where the coupling involving the CT states also exhibits high values (Table 3). However, a longitudinal displacement along the x-axis leads to a significant decrease in the couplings, nearly vanishing at ≈ 2 meV for model MOF-C. The electronic coupling decreases by ≈−17 meV when comparing the MOF-A to the MOF-B configuration.

We note that the superexchange coupling may interfere destructively, potentially leading to complete cancellation through the leading configurations. It is worth noting that E_{CT} is very sensitive to the packing configuration of the monomer in a dimer (Table 3).

Table 2. Relative shift along x, y and z axes in Å for dimer pairs of PEN as obtained from the crystal structure and MOF dimer models (see Figure 5).

Dimer pair	Long axis (Δx)	short axis (Δy)	$\pi - \pi$ (Δz)
PEN-A	1.81	5.73	7.58
PEN-B	1.72	6.72	5.98
PEN-C	1.78	3.21	5.75
MOF-A	1.81	1.21	3.58
MOF-B	6.87	1.05	3.58
MOF-C	9.48	1.18	3.58

Table 3. The effective electronic coupling J_{eff} between Frenkel excitation and multi-excitation of PEN and MOF dimer models. Experimental values for the pentacene thin film are E_{S1} = 1.83 eV and E_{T1} = 0.86 eV.[50] From UV/Vis measurements of ZnPn we extract E_{S1} = 2.03 eV.

	E_{S1}[eV]	E_{CT}[eV]	E_{T1}[eV]	J_{eff}[meV]
PEN-A	1.79	2.03	0.77	5.49
PEN-B	1.79	2.09	0.77	0.72
PEN-C	1.79	2.08	0.77	16.80
MOF-A	1.83	2.03	0.58	21.53
MOF-B	1.83	2.12	0.58	3.2
MOF-C	1.83	2.80	0.58	2.2

2.3.3. Rate of Singlet Fission From Marcus Theory

To evaluate the feasibility of employing these dimers in organic photovoltaics, we have calculated the rate of formation of the multi-excitonic state K_{SF} using Equation (3). The reorganization energy and Gibbs free energy (ΔG) of charge transfer play a significant role in the Marcus approach. As expected, ΔG values are negative, indicating that the initial states are higher in energy than the final states. Considering that the reorganization energy of PEN is estimated to be in the range of 108–136 meV and in the MOF it is 116–201 meV, the reorganization energies vary between ∼ 30 and 80 meV for PEN and MOF models, respectively, for different configurations (cf. Figure S2, Supporting Information). As a result, K_{SF} varies by two orders of magnitude among various dimer configurations, see Figure 6.

Our findings suggest that a variation in the stacking geometry of the two molecules in the dimer can indeed have a substantial impact on the kinetics of the SF process, confirming the

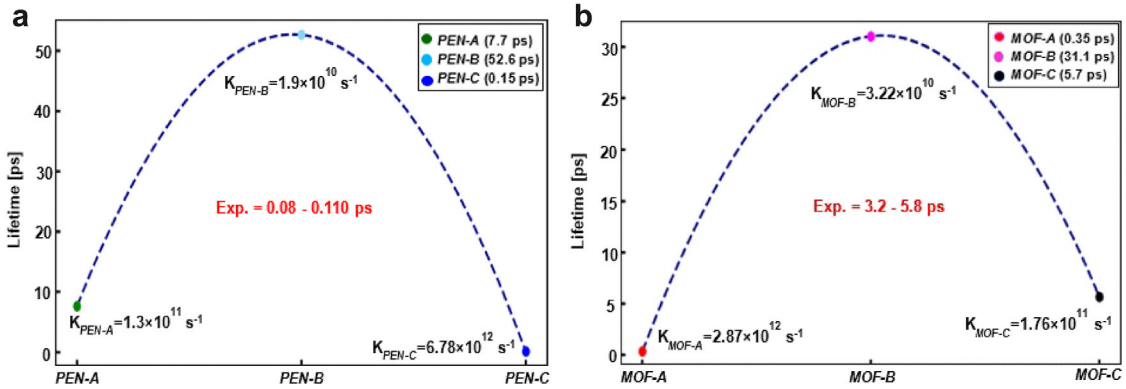

Figure 6. Singlet fission rates for PEN and MOF models. The rates were calculated using the Marcus rate equation.

expected influence of the intermolecular geometry.[51,52] It is worth noting that the variations in K_{SF} follow the trend determined by the one-electron coupling parameter J_{eff}, as shown in Table 3. In this context, PEN-C exhibits a high SF rate of ≈147 fs and possesses the largest coupling energy (≈16 meV). Conversely, the other two molecules exhibit negligible effective coupling values of 0.72 and 5.47 meV, accompanied by significantly longer time constants of ≈ 7–50 ps. The observed trend of SF rates (PEN-C > PEN-A > PEN-B) correlates closely with the trend identified for the effective coupling (Table 3). It is important to note that PEN-C and PEN-B possess very similar values of the $\pi - \pi$ distance (Table 2), yet they differ by nearly a factor of 10 in SF conversion rate. The highly favourable geometry for ultrafast SF, as exhibited by PEN-C can be rationalized by the computational results, specifically highlighting the electronic coupling between the S_1S_0 and ^{1}(TT) state. Hence, PEN-C is considered the geometry for the further analysis.

Considering the MOF models, we find that MOF-A shows the highest SF conversion, while MOF-B exhibits the lowest, thereby resulting in SF rates of 0.348 or 31.05 ps respectively. MOF-C shows a SF rate of 5.68 ps, a value consistent with experimental findings (exp: 3.2–5.8 ps). The SF rate constant decreases in the order: MOF-A (J_{eff} = 21.53 meV) > MOF-C (J_{eff} = 2.2 meV)>MOF-B (J_{eff} = 3.2 meV). Here, the trend of rates does not follow the effective coupling, but the reorganisation energy can explain the change in order. While MOF-B and C have similar effective couplings J_{eff}, MOF-B exhibits a higher reorganisation energy (λ =201 meV) than MOF-C (λ = 132 meV), slowing down the rate in MOF-B. In summary, we find that the dimer geometry of MOF-C results in the closest match between the calculated coupling strength and the experimental SF rate constant.

2.3.4. Excited State Dynamics

After reaching the S_1 state, three kinetically competitive excited-state deactivation pathways from S_1 to the ground state have to be considered: radiative (fluorescence) and non-radiative (SF and intersystem crossing (ISC)Methods) deactivation pathways.[53] These reaction channels have been explored through nonadiabatic excited-state dynamics simulation of materials, as their significance for SF has been well established. The kinetics of the rate constants for the reference compound PEN and MOF are depicted in Figure 7, which also incorporates available experimental data.

The multi-excitonic generation reaction (K_{SF}) unfolds several orders of magnitude faster than the competing fluorescence process (K_r), highlighting that the initial spectral features arise from S_0S_1, whereas features at later times are attributed to ^{1}(TT) and (T_1+T_1) in both materials. The decorrelated (T_1+T_1) state is mediated by spin mixing with a quintet correlated triplet pair ^{5}(TT). The energy of the lowest singlet excited state $E_{S_0S_1}$, has been determined as $E_{S_0S_1}$ = 1.79 and 1.83 eV for PEN and MOF respectively. Intermolecular coupling between the chromophores decreases $E_{S_0S_1}$ by ≈200 meV compared to that of respective monomers. The S_1 energy changes depend on the relative orientation in both materials, as differences in the crystal structures influence dipole-dipole interactions and orbital overlap between the chromophores, ultimately altering the electronic structure in the solid state.[54] The multi-exciton energies E_{TT}, for both materials have been calculated to be E_{TT} = 1.54 eV for PEN and 1.16 eV for MOF. Therefore, the corresponding energy gap of $|E_{S_0S_1}$-$E_{TT}|$ is determined to be 0.25 and 0.67 eV for PEN and MOF, respectively. Even slight changes in the S_1-T_1 energy gap can result in significant changes in the SF dynamics. The observed CT energies reveal that the CT state energy of MOF-C is ≈0.80 eV higher than that of PEN. As the energy of the virtual CT state decreases, the SF rate is expected to increase, but only until the CT state energy is nearly isoenergetic to or falls below that of the S_1 and ^{1}(TT) states. The time constant obtained from excited state dynamic analysis shows that PEN has comparable SF efficiency with a time constant of 147 fs, consistent with experimental results (exp.:80–110 fs). The MOF model features a slower triplet formation with a maximum of 31 ps for MOF-B and 5.68 ps for MOF-C which agrees best with the experimental values (exp: 3.2–5.8 ps). Regarding the relaxation to the ground state, the calculations indicate that TTA is unlikely — since E_{T2} exceeds $2E_{T1}$ by 0.77 eV, but they also reveal that the monomer exhibits a lifetime of 42 µs. We attribute this prolonged lifetime in part to the smaller reorganization energy for the MOF model (λ = 187 meV) compared to PEN (λ = 218 meV). This difference influences the vibrational overlap between the initial and final electronic states, which plays a critical role in determining the electronic transition rate (via the ISC rate calculation based on Fermi's golden rule). Such

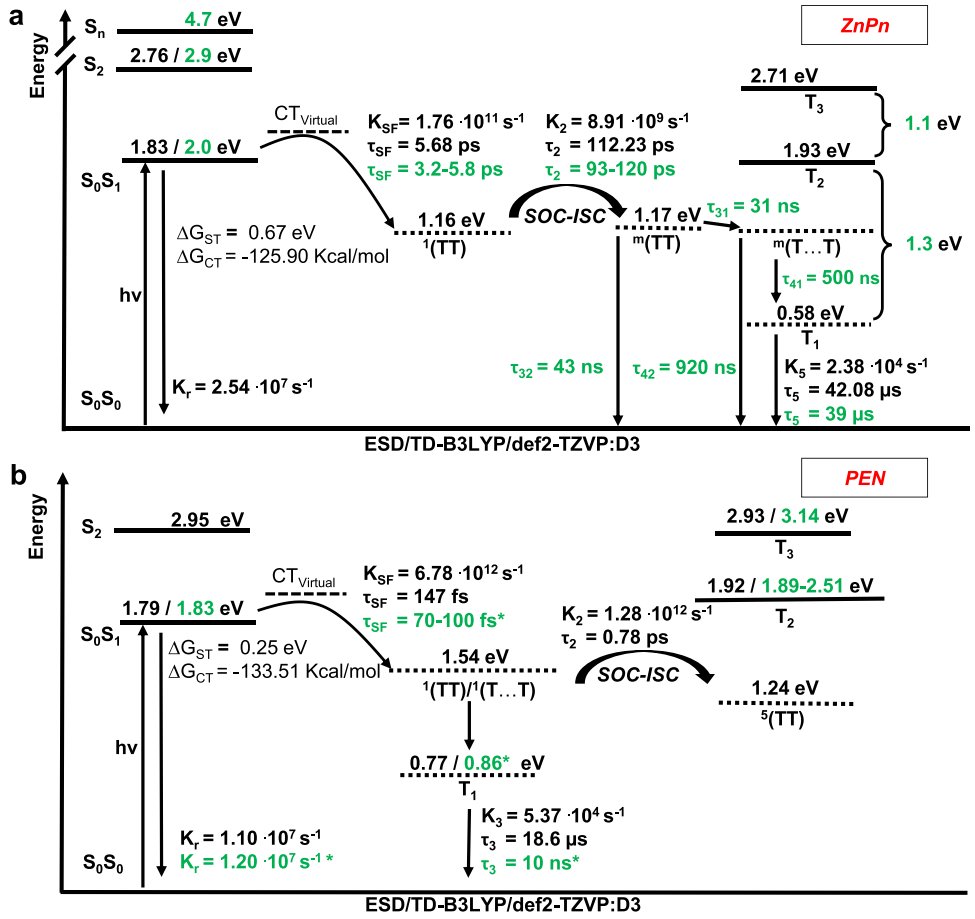

Figure 7. Reaction pathways illustrating the rates of radiative and non-radiative decay. a) Rates and energies of ZnPn and b) PEN obtained from experiments (green) and theoretical simulations (black) of the MOF-C and PEN-C dimer, respectively. Internal lifetimes are computed as $\tau = 1/K$. Experimental values with a star are taken from the literature.[11,14,50,56]

behavior is consistent with long-lived excited states and is likely a consequence of the distinct molecular structure. The excited state energies of both materials are depicted in Figure 7.

3. Discussion

From the findings of the TA experiments and our calculation, we motivate the kinetic model for PEN in the metal organic framework in Figure 7a. For comparison, the results for PEN are displayed in Figure 7b. They agree well with previously published studies.[4,37,55] We therefore believe that we can determine the relative orientation of the linkers in the MOF by comparing the calculated rates with experimental data. In the SURMOF we observe the generation of the triplet pair state $^1(T_1T_1)$ within a few picoseconds (4.9 ps) which is also the case for the model MOF-C (5.68 ps). This transition is promoted by the significantly polar CT character of the excited state through the superexchange mechanism. This slowdown in the rate compared to PEN (70–100 fs) can be rationalized by the higher CT state energy in the MOF model. The triplet signature peaking at 525 nm is formed from the intermediate state $^m(T_1T_1)$ with ≈119 ps. We assign this spectrum to the state ^{m}(TT) with the suggestion that m = 5 due to the slipped stacked geometry, which promotes the pathway via quintets to free triplet excitons.[4]

The transition from the ^{m}(TT) state to the ^{m}(T...T) state occurs over a timescale of ≈31 ns. Concurrently, there exists a competing decay pathway to the ground state with a timescale of 43 ns. Subsequently, uncorrelated triplets are generated on a timescale of 500 ns, with a loss channel characterized by a time constant of 920 ns. Finally, the triplet signature can be observed to decay to the ground state with a lifetime of 39 µs, which is an extremely promising improvement regarding the feasibility of SF materials. We account this increase in lifetime to the reduced TTA in our system and to the intrinsic stability of triplet states, due to the spin forbidden relaxation. A long triplet lifetime of the linker in the MOF has also been verified in our simulations. A reduction in triplet yield was observed in ZnPn, however, it is not nearly as pronounced as in the PEN thin film, where TTA is the dominating process, considering the fluences applied here. Regarding applicability, interdigitated bottom contacts can be attached to the SURMOF[57] to serve as electrodes. The conduction mechanism has already been investigated: a hopping-like charge transport was found for the system at hand,[21] but band-like transport is also possible in MOFs.[58,59] To function as an SF layer on top of photoactive semiconductor layer organic/organic

heterointerfaces as demonstrated in Ref. [60], may provide direct contact for energy transfer.

4. Conclusion

In summary, we have used a molecular engineering approach, exploiting the conformational freedom of MOFs to arrange pentacene moieties differently than in the PEN crystal. We characterized the ultrafast optical properties by experiment and theory. Clear evidence is found for triplet exciton generation. The change in geometric arrangement compared to the thin film structure has two major impacts: It slows down the triplet-pair generation by roughly two orders of magnitude, but at the same time the triplet lifetime is extended by almost four orders. The ability to achieve such novel molecular arrangements inaccessible in pure organic crystals significantly enhances the SF energetics. We find that manipulation of the π–π stacking distance is pivotal for optimizing intermolecular coupling in SF and will inform the design of next-generation MOF-based materials.

5. Methods Section

Sample Fabrication: The SURMOF (ZnPn) structure with Zn as metal nodes and the PEN linker as phenylcarboxylate substituted pentacene at 6- and 13-positions, were prepared by a spin-coating layer-by-layer method on quartz substrates, which is described elsewhere in more detail.[21] The PEN linker was synthesized according to literature.[21] The film thickness was controlled by the number of spin-coating cycles, which amounts to 85 nm for 75 cycles in our case. For comparison neat PEN thin films were fabricated by thermal evaporation at a base pressure of 1.9×10^{-9} mbar and a growth rate of 6 Å min^{-1}. Both samples were sealed under nitrogen atmosphere with a second glass to minimise possible effects due to photo-degradation.

UV/Vis and TA Spectroscopy: For steady-state UV/Vis spectroscopy a UV-2600i Shimadzu spectrometer was used. Transient absorption measurements were carried out with commercially available setups for short and long timescales (HELIOS and EOS, Ultrafast Systems). The output of a Ti:sapphire amplifier (Coherent Astrella) at 800 nm and a repetition rate of 4 kHz was used in a commercial optical parametric amplifier (TOPAS Prime, Light Conversion) to create the excitation pulse. The autocorrelation of the excitation pulse centred at 605 nm was ≈47 fs assuming a Gaussian pulse shape, measured with a commercial autocorrelator (pulseCheck, APE). For fs-TA a supercontinuum with a spectral range of 320–800 nm was created by focusing the Ti:sapphire output into a CaF_2 crystal. By focusing on a sapphire crystal instead, a supercontinuum was created ranging from 820 to 1500 nm. The delay of up to 8 ns was controlled by a motorised delay stage. To observe longer dynamics on time scales up to 200 µs, an electronically operated delay was employed. In this case, an external laser system (Leukos) generates a white light spectrum from 350 to 900 nm. The cross-correlation for this setup was ≈350 ps.

The samples were excited with pulse energies of 50 nJ up to 3000 nJ corresponding to 4244 µJ/ cm^2, and the polarization of the pump beam was set parallel to that of the probe beam. Pump and probe beam were focused with parabolic mirrors and were estimated to be 300 and 200 µm at the sample position in diameter, respectively. Since we measured ΔA, PIA has positive signal values and stimulated emission (SE) and ground state bleaching (GSB) have negative signal values. The open-source software Glotaran was used for global analysis of the TA data.[61]

Computational Methods: To elucidate the mechanism of SF we employed a methodology based on density functional theory (DFT). Specifically, the equilibrium structures of singlet ground (S0) and the first triplet (T_1) state of the systems were computed using Density functional theory (DFT) using the B3LYP hybrid exchange-correlation functional.[62–65] Singlet (S) – Triplet (T) adiabatic energy differences and T-T couplings were computed using ground state DFT (unrestricted wave functions were employed for triplets), which is referred to as ΔDFT. To analyse the structural minima harmonic vibrational frequencies were computed using the Aoforce program implemented in Turbomole 7.4.1 program. To assess the energetic criterion for singlet fission, vertical excitations and excited state geometry optimizations were computed using time-depended density functional theory (TD-DFT).[66] Throughout, the valence triple zeta basis set with polarization functions (d,p) (TZVP) was chosen.[67] Dispersion interactions were incorporated using Grimme's empirical dispersion correction (D3-Correction).[68] All optimizations were conducted without any symmetry constraints, the point group symmetry was identified as D_{2h} for Pentacene (PEN), and C_i for the Pentacene-MOF models (MOF) with D_2 and C_i symmetries determined to be the minimum energy structures for PEN and MOF respectively. All DFT/B3LYP and TD-B3LYP calculations were performed using Turbomole 7.4.1 program.[69] The electronic couplings for SF were calculated using the methodology described by Berkelbach et al.[70] for the superexchange mechanism,

$$J_{\text{eff}} = \langle S_1\, S_0^1 | \hat{V} | T_1\, T_1^1 \rangle = \langle S_1\, S_0^1 | \hat{H}_{\text{el}} | T_1\, T_1^1 \rangle - \frac{2(V_{LL} V_{LH} - V_{HH} V_{HL})}{E_{\text{CT}} - E_{\text{TT}} + E_{\text{CT}} - E_{S_1}} \quad (2)$$

In this expression, the first term of the right-hand side accounts for the contribution of the direct channel to the overall SF coupling while the second term accounts for the charge-transfer mediated superexchange coupling mechanism. The first term will be ignored in the subsequent analysis since the direct two-electron coupling $\langle S_1 S_0^1 | \hat{H}_{el} | T_1 T_1^1 \rangle$ is assumed to be small compared to the four one-electron couplings, V_{if}.[71,72] V_{LH} is the Fock matrix element between the LUMO in the donor and the HOMO in the acceptor, and the other matrix elements were defined similarly. E_{CT} and E_{TT} are the energy of the charge transfer states and of TT [≈2E (T1)], respectively. The rate constant for the transformation of the locally excited state into the multiexcitonic ^{1}(TT) state can be calculated as,

$$k_{SF} = \frac{2\pi}{\hbar} |J_{\text{eff}}|^2 \frac{1}{\sqrt{4\pi \lambda_{if} k_B T}} e^{-\frac{(\Delta G_{if} + \lambda_{if})^2}{4\lambda_{if} k_B T}} \quad (3)$$

Here, λ is the reorganization energy, and ΔG_{if} is the Gibbs free energy difference between the initial and final states i.e, $\Delta G_{if} = E_{S_0 S_1} - E_{TT}$. Finally, the rate of intersystem crossing K_{ISC} and fluorescence K_r were benchmarked using the ESD module implemented by Orca 5.O.4 program package.[66] The reliability of our

calculations was verified by comparing them with the available experimental values of PEN demonstrating excellent agreement between the experimental and computed values (cf. Table S1, Supporting Information).

Supporting Information

Supporting Information is available from the Wiley Online Library or from the author.

Acknowledgements

Funding by the German Research Foundation (DFG) through the Germany's Excellence Strategy 2082/1-390761711 is gratefully acknowledged. M.R. and P.T. acknowledge support by the DFG via the DFG project TE479/6-1. P.K. acknowledges support from DFG through the collaborative research center CRC 1249 "N-Heteropolycycles as Functional Materials" (Project Number 281029004- SFB 1249).

Open access funding enabled and organized by Projekt DEAL.

Conflict of Interest

The authors declare no competing interests.

Author Contributions

P.T. and W.W. oversaw the project. P.L. synthesized the PEN dicarboxylic acid. Z.X. fabricated the SURMOFs. C.H. fabricated the neat PEN thin films. Transient absorption spectroscopy was carried out by M.R. and P.V.K. M.R. carried out data analysis. Simulations were carried out by M.J.K. The paper was written by M.R. and M.J.K. with equal contribution and with contributions from P.V.K., W.W. and P.T. All authors contributed in the project discussions and production of the final manuscript.

Data Availability Statement

The data and code that support the findings of this study are available from the corresponding authors upon request.

Keywords

light harvesting, metal–organic framework, pentacene, singlet fission, transient absorption

Received: September 10, 2025
Revised: January 7, 2026
Published online:

[1] M. C. Hanna, A. J. Nozik, *J. Appl. Phys.* **2006**, *100*, 074510.
[2] W. Shockley, H. J. Queisser, *J. Appl. Phys.* **2004**, *32*, 510.
[3] M. J. Y. Tayebjee, S. N. Sanders, E. Kumarasamy, L. M. Campos, M. Y. Sfeir, D. R. McCamey, *Nat. Phys.* **2017**, *13*, 182.
[4] D. Lubert-Perquel, E. Salvadori, M. Dyson, P. N. Stavrinou, R. Montis, H. Nagashima, Y. Kobori, S. Heutz, C. W. M. Kay, *Nat. Commun.* **2018**, *9*, 4222.
[5] S. R. E. Orsborne, J. Gorman, L. R. Weiss, A. Sridhar, N. A. Panjwani, G. Divitini, P. Budden, D. Palecek, S. T. J. Ryan, A. Rao, R. Collepardo-Guevara, A. H. El-Sagheer, T. Brown, J. Behrends, R. H. Friend, F. Auras, *J. Am. Chem. Soc.* **2023**, *145*, 5431.
[6] N. Monahan, X.-Y. Zhu, *Annu. Rev. Phys. Chem.* **2015**, *66*, 601.
[7] S. Khan, S. Mazumdar, *J. Phys. Chem. Lett.* **2017**, *8*, 5943.
[8] R. D. Pensack, E. E. Ostroumov, A. J. Tilley, S. Mazza, C. Grieco, K. J. Thorley, J. B. Asbury, D. S. Seferos, J. E. Anthony, G. D. Scholes, *J. Phys. Chem. Lett.* **2016**, *7*, 2370.
[9] K. Miyata, F. S. Conrad-Burton, F. L. Geyer, X.-Y. Zhu, *Chem. Rev.* **2019**, *119*, 4261.
[10] E. Frankevich, V. Lesin, A. Pristupa, *Chem. Phys. Lett.* **1978**, *58*, 127.
[11] M. W. B. Wilson, A. Rao, J. Clark, R. S. S. Kumar, D. Brida, G. Cerullo, R. H. Friend, *J. Am. Chem. Soc.* **2011**, *133*, 11830.
[12] R. D. Pensack, A. J. Tilley, C. Grieco, G. E. Purdum, E. E. Ostroumov, D. B. Granger, D. G. Oblinsky, J. C. Dean, G. S. Doucette, J. B. Asbury, Y.-L. Loo, D. S. Seferos, J. E. Anthony, G. D. Scholes, *Chem. Sci.* **2018**, *9*, 6240.
[13] C. P. Theurer, M. Richter, D. Rana, G. Duva, D. Lepple, A. Hinderhofer, F. Schreiber, P. Tegeder, K. Broch, *J. Phys. Chem. C* **2021**, *125*, 23952.
[14] A. D. Poletayev, J. Clark, M. W. B. Wilson, A. Rao, Y. Makino, S. Hotta, R. H. Friend, *Adv. Mater.* **2014**, *26*, 919.
[15] I. Paci, J. C. Johnson, X. Chen, G. Rana, D. Popović, D. E. David, A. J. Nozik, M. A. Ratner, J. Michl, *J. Am. Chem. Soc.* **2006**, *128*, 16546.
[16] J. C. Johnson, A. J. Nozik, J. Michl, *Acc. Chem. Res.* **2013**, *46*, 1290.
[17] J. T. Blaskovits, M. Fumanal, S. Vela, C. Corminboeuf, *Chem. Mat.* **2020**, *32*, 6515.
[18] M. Nakano, S. Ito, T. Nagami, Y. Kitagawa, T. Kubo, *J. Phys. Chem. C* **2016**, *120*, 22803.
[19] R. D. Pensack, G. E. Purdum, S. M. Mazza, C. Grieco, J. B. Asbury, J. E. Anthony, Y.-L. Loo, G. D. Scholes, *J. Phys. Chem. C* **2022**, *126*, 9784.
[20] X. Liu, M. Kozlowska, T. Okkali, D. Wagner, T. Higashino, G. Brenner-Weiß, S. M. Marschner, Z. Fu, Q. Zhang, H. Imahori, S. Bräse, W. Wenzel, C. Wöll, L. Heinke, *Angew. Chem. Int. Ed.* **2019**, *58*, 9590.
[21] R. Haldar, M. Kozlowska, M. Ganschow, S. Ghosh, M. Jakoby, H. Chen, F. Ghalami, W. Xie, S. Heidrich, Y. Tsutsui, J. Freudenberg, S. Seki, I. A. Howard, B. S. Richards, U. H. F. Bunz, M. Elstner, W. Wenzel, C. Wöll, *Chem. Sci.* **2021**, *12*, 4477.
[22] R. Hesse, W. Hofberger, H. Bässler, *Chem. Phys.* **1980**, *49*, 201.
[23] R. He, N. G. Tassi, G. B. Blanchet, A. Pinczuk, *Appl. Phys. Lett.* **2005**, *87*, 103107.
[24] T. Jentzsch, H. Juepner, K.-W. Brzezinka, A. Lau, *Thin Solid Films* **1998**, *315*, 273.
[25] A. Hinderhofer, U. Heinemeyer, A. Gerlach, S. Kowarik, R. M. J. Jacobs, Y. Sakamoto, T. Suzuki, F. Schreiber, *J. Chem. Phys.* **2007**, *127*, 194705.
[26] M. W. B. Wilson, A. Rao, B. Ehrler, R. H. Friend, *Acc. Chem. Res.* **2013**, *46*, 1330.
[27] H. Yamagata, J. Norton, E. Hontz, Y. Olivier, D. Beljonne, J. L. Brédas, R. J. Silbey, F. C. Spano, *J. Chem. Phys.* **2011**, *134*, 204703.
[28] A. Rao, M. W. B. Wilson, S. Albert-Seifried, R. Di Pietro, R. H. Friend, *Phys. Rev. B* **2011**, *84*, 195411.
[29] C. K. Yong, A. J. Musser, S. L. Bayliss, S. Lukman, H. Tamura, O. Bubnova, R. K. Hallani, A. Meneau, R. Resel, M. Maruyama, S. Hotta, L. M. Herz, D. Beljonne, J. E. Anthony, J. Clark, H. Sirringhaus, *Nat. Commun.* **2017**, *8*, 15953.
[30] H. Marciniak, M. Fiebig, M. Huth, S. Schiefer, B. Nickel, F. Selmaier, S. Lochbrunner, *Phys. Rev. Lett.* **2007**, *99*, 176402.
[31] N. V. Korovina, N. F. Pompetti, J. C. Johnson, *J. Chem. Phys.* **2020**, *152*, 040904.
[32] S. N. Sanders, A. B. Pun, K. R. Parenti, E. Kumarasamy, L. M. Yablon, M. Y. Sfeir, L. M. Campos, *Chem* **2019**, *5*, 1988.
[33] J. Zirzlmeier, D. Lehnherr, P. B. Coto, E. T. Chernick, R. Casillas, B. S. Basel, M. Thoss, R. R. Tykwinski, D. M. Guldi, *Proc. Natl. Acad. Sci. U.S.A.* **2015**, *112*, 5325.
[34] S. N. Sanders, E. Kumarasamy, A. B. Pun, M. T. Trinh, B. Choi, J. Xia, E. J. Taffet, J. Z. Low, J. R. Miller, X. Roy, X.-Y. Zhu, M. L. Steigerwald, M. Y. Sfeir, L. M. Campos, *J. Am. Chem. Soc.* **2015**, *137*, 8965.

[35] M. T. Trinh, A. Pinkard, A. B. Pun, S. N. Sanders, E. Kumarasamy, M. Y. Sfeir, L. M. Campos, X. Roy, X.-Y. Zhu, *Sci. Adv.* **2017**, *3*, e1700241.
[36] R. Ringström, F. Edhborg, Z. W. Schroeder, L. Chen, M. J. Ferguson, R. R. Tykwinski, B. Albinsson, *Chem. Sci.* **2022**, *13*, 4944.
[37] I. Papadopoulos, J. Zirzlmeier, C. Hetzer, Y. J. Bae, M. D. Krzyaniak, M. R. Wasielewski, T. Clark, R. R. Tykwinski, D. M. Guldi, *J. Am. Chem. Soc.* **2019**, *141*, 6191.
[38] K. Kuroda, K. Yazaki, Y. Tanaka, M. Akita, H. Sakai, T. Hasobe, N. V. Tkachenko, M. Yoshizawa, *Angew. Chem. Int. Ed.* **2019**, *58*, 1115.
[39] P. V. Kolesnichenko, M. Hertzog, F. Hainer, D. D. M. Galindo, F. Deschler, J. Zaumseil, T. Buckup, *J. Phys. Chem. C* **2024**, *128*, 1496.
[40] A. J. Musser, J. Clark, *Annu. Rev. Phys. Chem.* **2019**, *70*, 323.
[41] A. Rao, R. H. Friend, *Nat. Rev. Mater.* **2017**, *2*, 17063.
[42] W. Kim, N. A. Panjwani, K. Krishnapriya, K. Majumder, J. Dasgupta, R. Bittl, S. Patil, A. J. Musser, *Cell Rep. Phys. Sci.* **2024**, *5*, 102045.
[43] G. He, E. M. Churchill, K. R. Parenti, J. Zhang, P. Narayanan, F. Namata, M. Malkoch, D. N. Congreve, A. Cacciuto, M. Y. Seir, L. M. Campos, *Nature Commun.* **2023**, *14*, 6080.
[44] W.-L. Chan, M. Ligges, X.-Y. Zhu, *Nat. Chem.* **2012**, *4*, 840.
[45] N. A. Pace, D. H. Arias, D. B. Granger, S. Christensen, J. E. Anthony, J. C. Johnson, *Chem. Sci.* **2018**, *9*, 3004.
[46] C.-H. Yang, C.-P. Hsu, *J. Physical Chem. Lett.* **2015**, *6*, 1925.
[47] F. Mirjani, N. Renaud, N. Gorczak, F. C. Grozema, *J. Phys. Chem. C* **2014**, *118*, 14192.
[48] C. C. Mattheus, A. B. Dros, J. Baas, A. Meetsma, J. L. d. Boer, T. T. M. Palstra, *Acta Crystallogr. C* **2001**, *57*, 939.
[49] C. H. Yang, C. P. Hsu, *J. Phys. Chem. Lett.* **2015**, *6*, 1925.
[50] J. Burgos, M. Pope, C. E. Swenberg, R. R. Alfano, *Phys. Status Solidi B* **1977**, *83*, 249.
[51] M. A. Castellanos, P. Huo, *J. Phys. Chem. Lett.* **2017**, *8*, 2480.
[52] N. Renaud, P. A. Sherratt, M. A. Ratner, *J. Phys. Chem. Lett.* **2013**, *4*, 1065.
[53] M. Fujitsuka, C. Lu, T. Iwamoto, E. Kayahara, S. Yamago, T. Majima, *J. Phys. Chem. A* **2014**, *118*, 4527.
[54] N. J. Hestand, F. C. Spano, *Acc. Chem. Res.* **2017**, *50*, 341.
[55] P. M. Greißel, D. Thiel, H. Gotfredsen, et al., *Angew. Chem. Int. Ed.* **2024**, *63*, e202315064.
[56] N. Nijegorodov, V. Ramachandran, D. Winkoun, *Spectrochim. Acta A Mol. Biomol. Spectrosc.* **1997**, *53*, 1813.
[57] X. Liu, M. Kozlowska, T. Okkali, et al., *Ange. Chem. Int. Ed.* **2019**, *58*, 9590.
[58] R. Dong, P. Han, H. Arora, et al., *Nature Mat.* **2018**, *17*, 1027.
[59] S. Fu, E. Jin, H. Hanayama, et al., *J. Am. Chem. Soc.* **2022**, *144*, 7489.
[60] A. Chandresh, X. Liu, C. Wöll, L. Heinke, *Adv. Sci.* **2021**, *8*, 2001884.
[61] J. J. Snellenburg, S. Laptenok, R. Seger, K. M. Mullen, I. H. M. van Stokkum, *J. Stat. Softw.* **2012**, *49*, 1.
[62] A. D. Becke, *Phys. Rev. A* **1988**, *38*, 3098.
[63] A. D. Becke, *J. Chem. Phys.* **1993**, *98*, 5648.
[64] L. Wilk A N, D. M. Nusair, *J. Phys.* **1980**, *58*, 3812.
[65] C. Lee, W. Yang, R. G. Parr, *Phys. Rev. B* **1988**, *37*, 785.
[66] F. Neese, F. Wennmohs, U. Becker, C. Riplinger, *J. Chem. Phys.* **2020**, *152*, 224108.
[67] F. Weigend, R. Ahlrichs, *Phys. Chem. Chem. Phys.* **2005**, *7*, 3297.
[68] S. Grimme, J. Antony, S. Ehrlich, H. Krieg, *J. Chem. Phys.* **2010**, *132*, 154104.
[69] *Turbomole Program Package for Ab Initio Electronic Structure Calculations USER's MANUAL*, **2018**.
[70] T. C. Berkelbach, M. S. Hybertsen, D. R. Reichman, *J. Chem. Phys.* **2013**, *138*, 114103.
[71] Y. J. Bae, J. A. Christensen, G. Kang, et al., *J. Chem. Phys.* **2019**, *151*, 044501.
[72] S. Ito, T. Nagami, M. Nakano, *J. Phys. Chem. A* **2016**, *120*, 6236.